

Coexistence of planar and aplanar rotations in ^{195}Tl J. Peng^{a,*}, Q.B. Chen^{b,*}^a Department of Physics, Beijing Normal University, Beijing 100875, China^b Physik-Department, Technische Universität München, D-85747 Garching, Germany

ARTICLE INFO

Article history:

Received 6 January 2020

Received in revised form 9 May 2020

Accepted 11 May 2020

Available online 14 May 2020

Editor: W. Haxton

ABSTRACT

The chirality suggested for the doublet bands B2 and B2a in ^{195}Tl in $A \sim 190$ region is reexamined. The potential-energy curves and the configurations together with the deformation parameters are obtained by the constrained covariant density functional theory. The corresponding experimental energy spectra, energy differences between doublet bands, and the available $B(M1)/B(E2)$ values are investigated by the fully quantal particle rotor model. Analysis on the basis of the angular momentum components, the K -plots, and the azimuthal plots suggest a planar rotation interpretation for the bands B2 and B2a. Hence, it coexists with the aplanar rotation in the other doublet bands B4 and B4a in ^{195}Tl .

© 2020 The Author(s). Published by Elsevier B.V. This is an open access article under the CC BY license (<http://creativecommons.org/licenses/by/4.0/>). Funded by SCOAP³.

The phenomenon of spontaneous chiral symmetry breaking is a subject of general interest. In atomic nuclear physics, it exists in triaxially deformed nucleus with high- j valence particle(s) and high- j valence hole(s) [1]. Due to the angular momentum coupling between particle(s), hole(s), and core, the total angular momentum vector may lie outside the three principal planes in the intrinsic frame and hence forms as aplanar rotation. In the laboratory frame, such kind of aplanar rotation could give rise to a pair of nearly degenerate $\Delta I = 1$ bands with the same parity, i.e., chiral doublet bands [1]. With the extensive efforts over twenty years, this exotic collective mode has become a general phenomenon over the nuclear chart. More than 50 chiral candidates were found in odd-odd, odd- A , and even-even nuclei that spread over $A \sim 80, 100, 130$, and 190 mass regions. For more details, see reviews [2–8] and very recent data tables [9].

As an important extension of nuclear chirality, the phenomenon of multiple chiral doublets ($M\chi D$), i.e., having multiple pairs of chiral doublet bands in a single nucleus, was predicted and explored extensively by the state-of-art covariant density functional theory (CDFT) [10–16] and observed in ^{133}Ce [17], ^{103}Rh [18], ^{78}Br [19], ^{136}Nd [20], ^{195}Tl [21], and ^{135}Nd [22]. These observations confirm the existence of triaxial shapes coexistence [10, 17, 20–22], and reveal the stability of chiral geometry against the increasing of intrinsic excitation energy [18, 23–25] and octupole correlations [19].

As mentioned above, most of observations of chiral doublet bands concentrate on the medium mass regions. Therefore, there

is a fundamental goal to hunt for new candidates with chirality or $M\chi D$ in new mass regions. On the one hand, the possibility of chiral doublet bands or $M\chi D$ has been investigated in ^{60}Ni [26] and $^{54,56,57,58,59,60}\text{Co}$ [16] in $A \sim 60$ mass region to open the lighter mass area of chirality. On the other hand, for the heavier mass region, several high-spin states of chirality have been reported in $A \sim 190$ nuclei [21, 27–31].

In Ref. [21], the high-spin states in ^{195}Tl were reported. Of which, two pairs of doublet bands were assigned to be built on two different quasi-particle configurations. One of them is labeled as bands B4 and B4a based on a five-quasiparticle configuration $\pi i_{13/2} \otimes \nu i_{13/2}^{-3}(pf)^{-1}$, and the other one bands B2 and B2a based on a three-quasiparticle configuration $\pi h_{9/2} \otimes \nu i_{13/2}^{-2}$. Based on the systematics of various experimental observable in $^{191,193,194,195}\text{Tl}$ isotopes and the triaxial shapes predicted by the total Routhian surface (TRS) calculations, it was concluded that both of them are chiral bands. In details, for bands B4 and B4a, the energies difference between doublets are small (average separation of 25 keV) and the $B(M1)/B(E2)$ ratios of the doublet bands are similar. These features do indeed fulfill the hallmarks of chiral doublet bands [1].

For bands B2 and B2a, however, as shown in Fig. 1, their energy differences (larger than 500 keV) are much larger than the typical value 200–300 keV of chiral doublet bands [9] and their $B(M1)/B(E2)$ ratios are not that similar on the magnitude and the staggering pattern as a function of spin. This looks as if the interpretation of chirality for this doublet bands was questionable. Does the aplanar rotation mode really exist in this doublet bands? To answer this question, a careful theoretical study of energy spectra, $B(M1)/B(E2)$ ratios, as well as angular momentum behaviors

* Corresponding authors.

E-mail addresses: jpeng@bnu.edu.cn (J. Peng), qbchen@pku.edu.cn (Q.B. Chen).

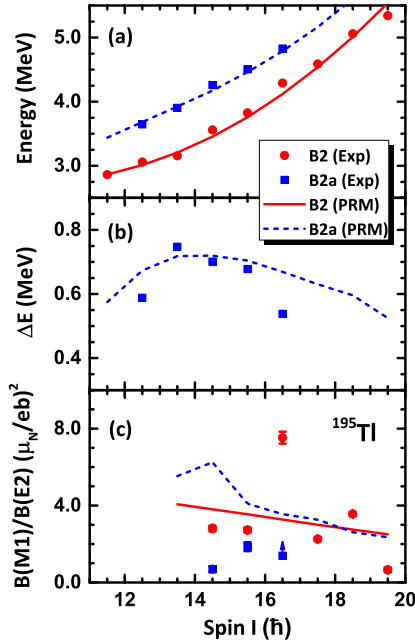


Fig. 1. (a) Experimental energy spectra as functions of spin for the bands B2 and B2a in ^{195}Tl in comparison with results calculated by PRM. (b) Experimental and theoretical energy differences between the doublet bands. (c) Experimental and theoretical $B(M1)/B(E2)$ ratios of bands B2 and B2a.

of the core, the proton $h_{9/2}$ particle, and the neutron $i_{13/2}^{-2}$ holes for bands B2 and B2a is necessary.

The aim of the present work is to investigate the chirality in doublet bands B2 and B2a in ^{195}Tl in a fully quantal model. As a quantal model coupling the collective rotation and the single-particle motions, the particle rotor model (PRM) has been widely used to describe the chiral doublet bands and achieved major successes [1,32–42]. In PRM, the total Hamiltonian is diagonalized with total angular momentum as a good quantum number, and the energy splitting and quantum tunneling between the doublet bands can be obtained directly. Furthermore, the basic inputs for PRM can be obtained from the microscopical constrained CDFT [10,17–19,22,43–45].

In this Letter, the constrained CDFT will be first carried out to obtain the deformation parameters for the assigned valence nucleon configurations. With these inputs, the PRM will be applied to study the energy spectra and the electromagnetic transition probabilities of the doublet bands B2 and B2a in ^{195}Tl , and to examine their angular momentum geometries.

The detailed formalism and numerical techniques of the adiabatic and configuration-fixed constrained CDFT calculation adopted in this work can be seen in Refs. [10,11] and references therein. In the calculations, the point-coupling density functional PC-PK1 [46] with a basis of 12 major oscillator shells is employed, while the pairing correlations are neglected for simplicity. The constrained calculations for $\langle \hat{Q}_{20}^2 + 2\hat{Q}_{22}^2 \rangle \sim \beta^2$ [10] and quantum number transformations [47] are carried out.

The potential-energy curves for ^{195}Tl calculated by adiabatic and configuration-fixed constrained CDFT are presented in Fig. 2(a). In comparison with the irregularities of energy curve in adiabatic constrained calculations, continuous and smooth energy curves for each configuration are yielded by the configuration-fixed constrained calculations. The obvious local minima are marked by stars and labeled by letters of the alphabet.

Two minima labeled as A and B in potential energy curve in Fig. 2(a) have appropriate triaxial deformation, but do not have suitable high- j particle-hole configurations for chirality. Here, state

A represents the ground state, with the deformation parameters ($\beta = 0.16$, $\gamma = 40.8^\circ$) and the valence nucleon configuration, as shown in Fig. 2(b), $\pi h_{9/2} \otimes \nu [i_{13/2}^{-4} (pf)^4]$. Although state B has the remarkable triaxial deformation, it has only a unpaired nucleon configuration $\pi 3s_{1/2}$ instead of necessary high- j particle-hole configuration. By keeping always two aligned neutrons in the fifth and sixth levels of the $i_{13/2}$ shell, and the other neutrons filling in the orbitals according to their energies, low-lying particle-hole excitation state C (the unpaired nucleon configuration $\pi h_{9/2} \otimes \nu i_{13/2}^{-2}$) are obtained as shown in Fig. 2(c). By exciting one proton occupying the $h_{9/2}$ orbital to the $i_{13/2}$ orbital and one neutron from the (pf) shell to the $i_{13/2}$ shell on the basis of ground state A, the configuration of state D (the unpaired nucleon configuration $\pi i_{13/2} \otimes \nu [i_{13/2}^{-1} (pf)^1]$) is obtained. Similarly, the unpaired nucleon configuration $\pi i_{13/2} \otimes \nu [i_{13/2}^{-3} (pf)^1]$, labeled E in Fig. 2(a), are obtained by exciting one $i_{13/2}$ neutron ($m_z \sim 9/2$) to a higher $i_{13/2}$ orbit ($m_z \sim 13/2$) on the basis of state D. In the subsequent calculations with the fixed configurations of C, D and E, the occupations of the valence nucleons are traced by the configuration-fixed constrained calculations [10]. The obtained results are presented in Figs. 2(a). Both minima C and D have deformation parameters β and γ suitable for chirality, which are C ($\beta = 0.16$, $\gamma = 45.6^\circ$) and D ($\beta = 0.16$, $\gamma = 42.6^\circ$). These two states have triaxial deformations as well as high- j particle-hole configurations that suitable for establishing chiral rotation. Therefore, the existence of chiral doublets or $M\chi D$ could be expected in ^{195}Tl .

It should be noted that the configuration $\pi h_{9/2} \otimes \nu i_{13/2}^{-2}$ suggested for the doublet bands B2 and B2a in ^{198}Tl in Ref. [21] corresponds to that of state C here shown in Fig. 2(a). The obtained deformation parameters are close to the one ($\beta = 0.15$, $\gamma = 39.0^\circ$) by TRS calculations [21]. To display more clearly, in Figs. 2(b) and (c), we show the single-particle energy levels of proton and neutron near the Fermi surface for the ground state A and state C, respectively. For the ground state A, we solve the Dirac equation by filling, in each step of the iteration, the proton and neutron levels according to their energies from the bottom of the well. As shown in Fig. 2(b), for the proton single-particle energy levels, there is always a particle sitting on the bottom of the $h_{9/2}$ shell. In comparison, there are four paired neutron holes sitting on the top of the $i_{13/2}$ shell. For the ground state, the proton has already played a role of high- j particle, but there is not high- j hole involved. For state C, two of the neutron holes align along the z -axis through one-particle-one-hole neutron excitation from the ($i_{13/2}$, $m_z \sim 9/2$) orbital to the higher ($i_{13/2}$, $m_z \sim 11/2$) orbital. This kind of excitation leads to the valence nucleon configuration with the form of $\pi h_{9/2} \otimes \nu i_{13/2}^{-2}$ shown in Fig. 2(c).

Subsequently, the PRM calculations with the configuration $\pi h_{9/2} \otimes \nu i_{13/2}^{-2}$ for the doublet bands B2 and B2a in ^{198}Tl are performed. As discussed above, the deformation parameters $\beta = 0.16$ and $\gamma = 45.6^\circ$ for this configuration at the bandhead were obtained from the configuration-fixed constrained CDFT calculations. The irrotational flow type of moment of inertia $\mathcal{J}_k = \mathcal{J}_0 \sin^2(\gamma - 2k\pi/3)$ with $\mathcal{J}_0 = 20.0 \text{ } \hbar^2/\text{MeV}$ and Coriolis attenuation factor $\xi = 0.95$ are adopted according to the experimental energy spectra. For the electromagnetic transitions, the empirical intrinsic quadrupole moment $Q_0 = (3/\sqrt{5\pi})R_0^2 Z\beta$, and gyromagnetic ratios for rotor $g_R = Z/A$ and for nucleons $g_{\pi(\nu)} = g_l + (g_s - g_l)/(2l + 1)$ ($g_l = 1(0)$ for protons (neutrons) and $g_s = 0.6g_s(\text{free})$) [48] are used.

The calculated energy spectra for the doublet bands B2 and B2a in ^{195}Tl are presented in Fig. 1(a), together with the corresponding data. The experimental energy spectra are reproduced excellently by the PRM calculations. Being a quantum model, PRM is able to reproduce the energy splitting for the whole observed spin region. It is seen in Fig. 1(b) that the trend for the ΔE between partner

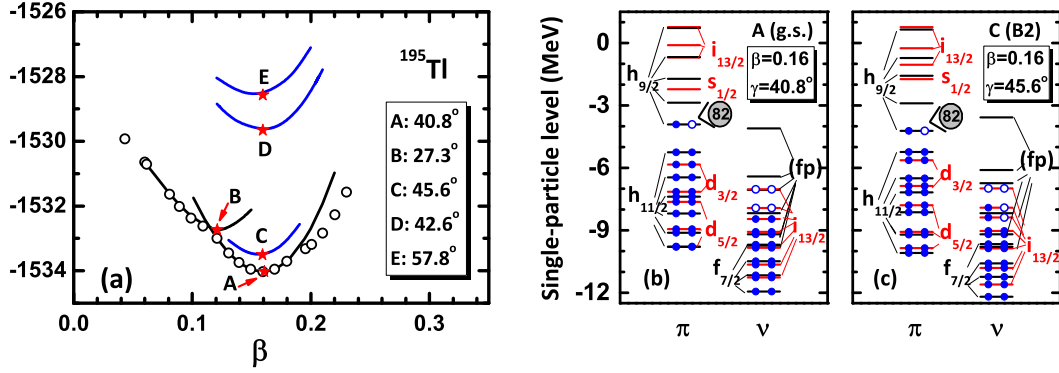


Fig. 2. (a) The potential-energy curves in adiabatic (open circles) and configuration-fixed (solid lines) constrained triaxial CDFT calculation with PC-PK1 for ^{195}Tl . The local minima in the energy surfaces for fixed configuration are represented as stars and labeled respectively as A, B, C, D, and E. (b) Single-proton (left column) and single-neutron (right column) levels near the Fermi surface in ^{195}Tl for the state A. (c) Same as (b) but for the state C.

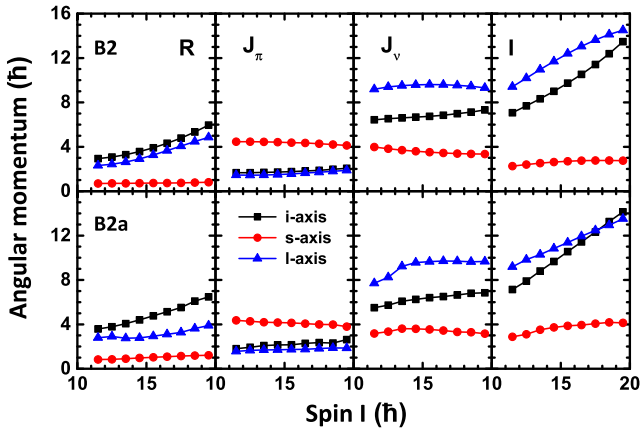


Fig. 3. The root mean square components along the short (*s*-axis, squares), intermediate (*i*-axis, circles), and long (*l*-axis, triangles) axes for the rotor, valence proton, valence neutrons, and total angular momenta as functions of spin calculated by PRM for the doublet bands B2 and B2a in ^{195}Tl .

bands is reproduced well. Namely, the ΔE increases firstly before $I = 14.5\hbar$, and then decreases. Furthermore, as mentioned above, the ΔE is considerably large. In detail, the minimum of ΔE is 588 keV, and the maximum is 747 keV; much larger than the typical value 200–300 keV of chiral doublet bands [9].

Besides the close excitation energies, another important characteristics of chirality is the similar behavior of the $B(M1)/B(E2)$ ratios for chiral pairs [1,9]. In Fig. 1(c), one has already observed the significant differences between the experimental $B(M1)/B(E2)$ of doublet bands, including the magnitudes and odd-even staggering pattern. As a comparison, the calculated $B(M1)/B(E2)$ values by PRM are also shown in Fig. 1(c). No obvious odd-even staggering of the $B(M1)/B(E2)$ values is presented, although an effect is apparent experimentally. Except for $I = 16.5\hbar$, the PRM calculations show a good agreement with the data for the band B2. For the band B2a, the PRM overestimates the experimental data. As discussed in Ref. [28] for the doublet bands in ^{198}Tl , a so-called residual proton-neutron interaction has an effect on the staggering behavior of $B(M1)/B(E2)$. Here, the discrepancies between the theoretical and experimental $B(M1)/B(E2)$ might be attributed to the fact that we here do not consider the proton-neutron interaction.

The consistency with the energy spectra of the doublet bands, together with the discrepancy between the theoretical $B(M1)/B(E2)$ and the data, motivate us to examine the angular momentum geometry microscopically. From the eigenfunctions calculated by PRM, one can calculate the expectation values of the squared angular momentum components along the short (*s*-), intermediate

(*i*-), and long (*l*-) axes for the rotor, valence proton, valence neutrons, and total angular momenta, which are shown in Fig. 3.

The asymmetric degree of the configuration $\pi h_{9/2} \otimes \nu i_{13/2}^{-2}$ will lead to considerable difference between angular momenta coming from the valence particle (along the *s*-axis) and holes (along the *l*-axis), and hence drives triaxial deformation to deviate away from maximal triaxiality $\gamma = 30^\circ$. This will in return influence the angular momentum geometry of the rotating system.

As shown in Fig. 3, for both bands B2 and B2a, the valence proton in the $h_{9/2}$ orbital contributes about $4.5\hbar$ to the angular momentum along the *s*-axis, while the valence neutron $i_{13/2}$ holes contribute to the angular momentum with $\sim 10\hbar$ mainly aligning along *l*-axis as a comparison. The neutron angular momentum comes mainly from the two aligned neutron holes in the middle of $i_{13/2}$ shell with $m_z \sim -11/2$ and $m_z \sim -9/2$. As a result, besides the substantial components in *l*-axis ($\sim 10\hbar$), the components along *i*-axis ($\sim 6\hbar$) and *s*-axis ($\sim 4\hbar$) are also non-negligible.

The angular momentum of collective core has largest component along the *i*-axis in the whole spin region, because it has the largest moment of inertia. It should be noted that for both bands, the rotor angular momenta exhibit also substantial contributions to the *l*-component. This is understood as reasons of triaxial deformation deviating far away from $\gamma = 30^\circ$ and the strong Coriolis effects. In details, for the adopted triaxiality $\gamma = 45.6^\circ$, the ratios among the moments of inertia for the three principal axes are $\mathcal{J}_i : \mathcal{J}_s : \mathcal{J}_l = 1.00 : 0.07 : 0.54$. Therefore, the collective angular momentum vector no longer tends to align purely along the intermediate axis, and this leads to the substantial contributions to the *l*-component. Moreover, the significant *l*-component of the neutron holes reproduces a strong Coriolis force to the rotor and drive it align along the *l*-axis to minimize the energy.

As a result of the angular momentum couplings among the rotor, valence proton, and valence neutron holes, the total angular momentum has large components along the *l*- and *i*-axes, while very small one along the *s*-axis. Such orientations form the angular momentum geometry of planar rotation in the *l*-*i* plane instead of chiral geometry of aplanar rotation.

To further understand the evolution of the angular momentum geometry with spin, in Fig. 4, the *K*-plots, i.e., *K*-distributions for the angular momentum on the *s*-, *i*-, and *l*-axes calculated by PRM for the doublet bands B2 and B2a in ^{195}Tl are displayed. As seen in the figures, for the whole observed spin region, the *K*-distributions of bands B2 and B2a remain almost unchanged.

For bands B2 and B2a, the peaks of K_s locate at $K_s = 0.5\hbar$ for the whole spin region. The peaks locating at the smallest K_s value indicate that the *s*-components of the proton particle and neutron holes are canceled each other out. Due to this canceling, the total

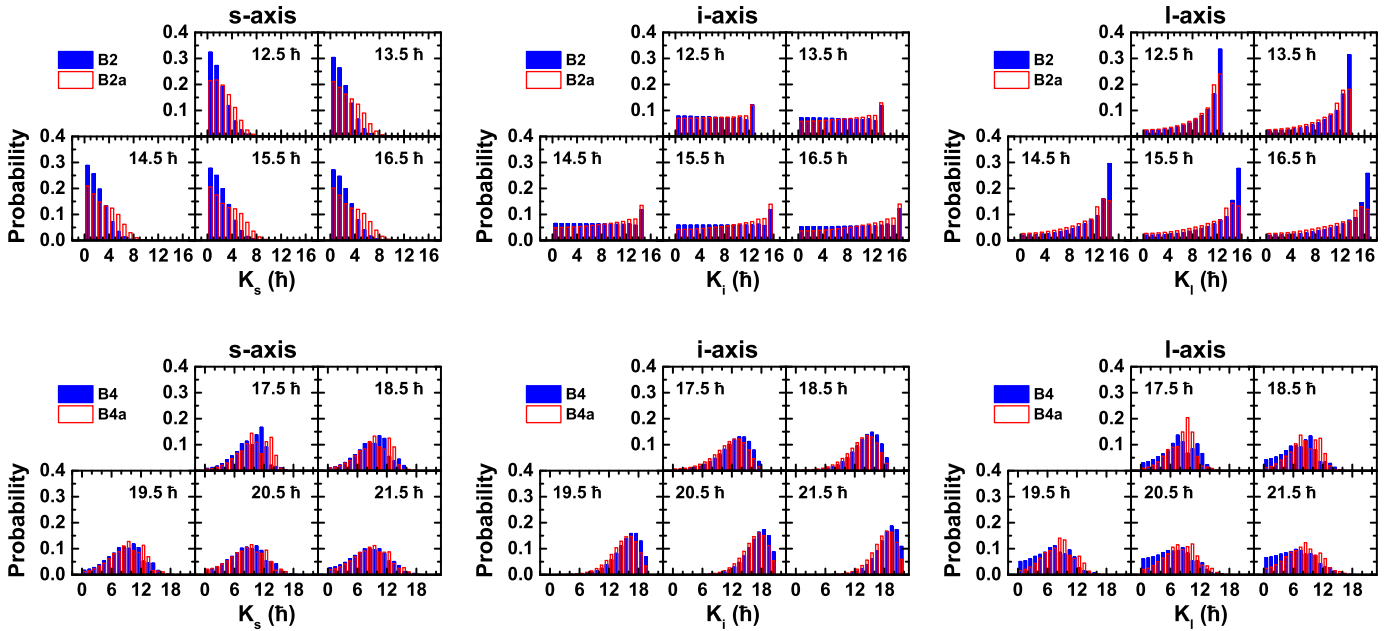


Fig. 4. The K -plots, i.e., K -distributions for the angular momentum on the short (s -), intermediate (i -), and long (l -) axes calculated by PRM for the doublet bands B2 and B2a as well as B4 and B4a in ^{195}Tl .

angular momentum has too small component along the s -axis to form the aplanar rotation.

The K_i -distributions of bands B2 and B2a are similar and spread widely. Due to the contribution from the neutron holes, there is a weak peak on the top of dispersive K_i -distributions which moves from $K_i = 12.5\hbar$ to $K_i = 16.5\hbar$ gradually with spin.

The K_l -distributions of bands B2 and B2a behave in a similar way, except that the value of peak of K_l distribution for band B2 is a bit larger than those for band B2a. Their peaks locate around the largest K_l value, mainly contributing from the two high- j neutron holes.

Therefore, the angular momenta for bands B2 and B2a always stay within the i - l plane. The appearance of static chirality or chiral vibration for bands B2 and B2a is not supported.

In order to visualize the angular momentum geometry in the intrinsic frame, the azimuthal plots [26,49–52], i.e., probability density profiles $\mathcal{P}(\theta, \varphi)$ for the orientation of the angular momentum on the (θ, φ) plane calculated by PRM are shown in Fig. 5 for the doublet bands B2 and B2a in ^{195}Tl at $I = 12.5$ – $16.5\hbar$. Here, θ is the angle between the total spin I and the s -axis, and φ is the angle between the projection of I onto the li -plane and the l -axis. As shown in Fig. 5, the azimuthal plots are symmetric with respect to $\varphi = 0^\circ$ due to the D_2 symmetry of triaxial shape. The maximum of the profiles is always located at $\theta = 90^\circ$. This is consistent with the very small s -component of the total spin as shown in Fig. 3, and rules out the possibility of the aplanar rotation interpretation.

For the whole observed spin region, the profiles for the orientation of the angular momentum for band B2 behave in a similar way. The most probable probability appears at $(\theta = 90^\circ, \varphi = 0^\circ)$. The profiles also show soft along the φ -direction, which is due to the competition from the i -component of the angular momentum from the rotor and neutron holes. This feature corresponds to a planar rotation within the i - l plane. Such orientation does not form a chiral geometry and no chirality is shown in band B2. This is consistent with the angular momentum components shown in Fig. 3 and K -distributions shown in Fig. 4.

For band B2a, its profile exhibits the similar features as band B2 one at $I = 12.5\hbar$, i.e., a peak at $(\theta = 90^\circ, \varphi = 0^\circ)$ and softness with respect to the φ -direction. With the increase of spin, the higher excitation energies and the stronger Coriolis force from

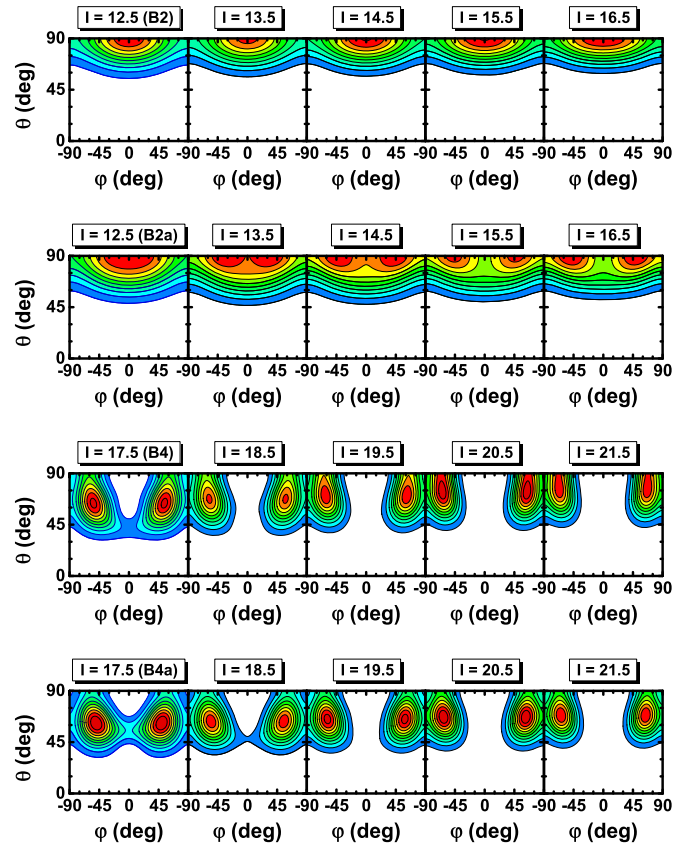


Fig. 5. The azimuthal plots, i.e., probability density profiles for the orientation of the angular momentum on the (θ, φ) plane calculated by PRM for the doublet bands B2 and B2a as well as B4 and B4a in ^{195}Tl .

the valence neutron holes and rotor drive the angular momentum to align gradually toward the i -axis. Two peaks appear, which are $(\theta = 90^\circ, \varphi \sim \pm 35^\circ)$ for $I = 13.5\hbar$, and φ increase gradually with spin. This further supports that the total angular momentum stays within the i - l plane. These features are quite similar as those

for the transverse wobbling shown in Refs. [51,52], only there the probability density at $\varphi = 0^\circ$ vanishes due to the anti-symmetric $n = 1$ wobbling phonon excitation. The non-vanished probability density at $\varphi = 0^\circ$ here is attributed to the significant i -component of the neutron holes angular momenta.

It should be mentioned that the same conclusion is obtained by PRM calculation based on ($\beta = 0.15$, $\gamma = 39^\circ$), which is predicted by TRS of band B2 in Ref. [21].

In addition, the same calculations were also made for the doublet bands B4 and B4a, and the results of K -plots and azimuthal plots are also shown in Fig. 4 and 5, respectively (noted that in Fig. 5 for bands B4 and B4a, the θ is defined as the angle between the total spin \mathbf{I} and the l -axis, and the φ is defined as the angle between the projection of total spin \mathbf{I} onto the s - m plane and the s -axis). It is clearly seen that these results support aplanar coupling of angular momenta for this pair of doublet bands. Namely, the K -distributions of the doublet bands B4 and B4a are similar. Furthermore, the peaks of the three K -distributions locate all at non-zero K -values, indicating that the total angular momentum has finite components along the three principal axes. Two peaks corresponding to aplanar orientations of the total angular momentum are found in the azimuthal plots for both of doublet bands at each spin. All of these features could be understood as a realization of static chirality, and hence give the small energy differences as the experiment shows. Therefore, the aplanar (bands B4 and B4a) and planar (bands B2 and B2a) rotations coexists in triaxially deformed nucleus ^{195}Tl .

In summary, the chirality suggested in doublet bands B2 and B2a in the odd- A ^{195}Tl in $A \sim 190$ region is reexamined by adopting the microscopic constrained CDFT and fully quantal PRM. The potential-energy curves, the configurations for doublet bands B2 and B2a of interest together with the corresponding deformation parameters are obtained by the adiabatic and configuration-fixed constrained CDFT calculations. The experimental energy spectra and energy differences between the doublet bands are reproduced well. The available $B(M1)/B(E2)$ values for the bands B2 and B2a are of different odd-even staggering pattern and exhibit different behaviors. Except for $I = 16.5\hbar$, the $B(M1)/B(E2)$ values for band B2 are reproduced well by the PRM calculations. The analysis based on the angular momentum components, the K -plots, and the azimuthal plots suggest that a planar rotation within the i - l plane for the bands B2 and B2a. The s -component of angular momentum contributed by the proton particle are canceled out by the neutron holes. The wobbling like mode for band B2a illuminates the richness of the rotation involving asymmetric nuclear shape.

Moreover, the aplanar rotation in bands B4 and B4a is confirmed by K -plots, and the azimuthal plots. Therefore, the planar and aplanar rotations coexist in triaxially deformed nucleus ^{195}Tl .

It is found that the asymmetric degree of the configuration $\pi h_{9/2} \otimes \nu i_{13/2}^{-2}$ and the neutron holes in the middle of $i_{13/2}$ shell favor the planar angular momentum geometry within the i - l plane instead of the traditional chiral geometry. The present results suggest that the asymmetric degree of the configuration in the nuclei of interest should be cautious in the future study of nuclear chirality. Definitely, further experimental efforts on the lifetime measurement of the states and the comparison of transition probabilities with the calculation to fully justify the rotational nature in ^{195}Tl is helpful.

Declaration of competing interest

The authors declare that they have no known competing financial interests or personal relationships that could have appeared to influence the work reported in this paper.

Acknowledgements

The authors thank Professor G. Mukherjee for providing the numerical data of experimental $B(M1)/B(E2)$ results and for reading of the manuscript, and thank Professor J. Meng for helpful discussions. This work is supported by the National Natural Science Foundation of China (NSFC) under Grants No. 11775026 and 11875027, and the Deutsche Forschungsgemeinschaft (DFG) and NSFC through funds provided to the Sino-German CRC110 "Symmetries and the Emergence of Structure in QCD" (DFG Grant No. TRR110 and NSFC Grant No. 11621131001).

References

- [1] S. Frauendorf, J. Meng, Nucl. Phys. A 617 (1997) 131.
- [2] J. Meng, S.Q. Zhang, J. Phys. G, Nucl. Part. Phys. 37 (2010) 064025.
- [3] J. Meng, Q.B. Chen, S.Q. Zhang, Int. J. Mod. Phys. E 23 (2014) 1430016.
- [4] R.A. Bark, E.O. Lieder, R.M. Lieder, E.A. Lawrie, J.J. Lawrie, S.P. Bvumbi, N.Y. Kheswa, S.S. Ntshangase, T.E. Madiba, P.L. Masiteng, et al., Int. J. Mod. Phys. E 23 (2014) 1461001.
- [5] J. Meng, P.W. Zhao, Phys. Scr. 91 (2016) 053008.
- [6] A. Raduta, Prog. Part. Nucl. Phys. 90 (2016) 241.
- [7] K. Starosta, T. Koike, Phys. Scr. 92 (2017) 093002.
- [8] S. Frauendorf, Phys. Scr. 93 (2018) 043003.
- [9] B.W. Xiong, Y.Y. Wang, At. Data Nucl. Data Tables 125 (2019) 193.
- [10] J. Meng, J. Peng, S.Q. Zhang, S.-G. Zhou, Phys. Rev. C 73 (2006) 037303.
- [11] J. Peng, H. Sagawa, S.Q. Zhang, J.M. Yao, Y. Zhang, J. Meng, Phys. Rev. C 77 (2008) 024309.
- [12] J.M. Yao, B. Qi, S.Q. Zhang, J. Peng, S.Y. Wang, J. Meng, Phys. Rev. C 79 (2009) 067302.
- [13] J. Li, S.Q. Zhang, J. Meng, Phys. Rev. C 83 (2011) 037301.
- [14] J. Li, Phys. Rev. C 97 (2018) 034306.
- [15] B. Qi, H. Jia, C. Liu, S.Y. Wang, Phys. Rev. C 98 (2018) 014305.
- [16] J. Peng, Q.B. Chen, Phys. Rev. C 98 (2018) 024320.
- [17] A.D. Ayangeakaa, U. Garg, M.D. Anthony, S. Frauendorf, J.T. Matta, B.K. Nayak, D. Patel, Q.B. Chen, S.Q. Zhang, P.W. Zhao, et al., Phys. Rev. Lett. 110 (2013) 172504.
- [18] I. Kuti, Q.B. Chen, J. Timár, D. Sohler, S.Q. Zhang, Z.H. Zhang, P.W. Zhao, J. Meng, K. Starosta, T. Koike, et al., Phys. Rev. Lett. 113 (2014) 032501.
- [19] C. Liu, S.Y. Wang, R.A. Bark, S.Q. Zhang, J. Meng, B. Qi, P. Jones, S.M. Wyngaardt, J. Zhao, C. Xu, et al., Phys. Rev. Lett. 116 (2016) 112501.
- [20] C.M. Petrache, B.F. Lv, A. Astier, E. Dupont, Y.K. Wang, S.Q. Zhang, P.W. Zhao, Z.X. Ren, J. Meng, P.T. Greenlees, et al., Phys. Rev. C 97 (2018) 041304(R).
- [21] T. Roy, G. Mukherjee, M.A. Asgar, S. Bhattacharyya, S. Bhattacharya, C. Bhattacharya, S. Bhattacharya, T.K. Ghosh, K. Banerjee, S. Kundu, et al., Phys. Lett. B 782 (2018) 768.
- [22] B.F. Lv, C.M. Petrache, Q.B. Chen, J. Meng, A. Astier, E. Dupont, P. Greenlees, H. Badran, T. Calverley, D.M. Cox, et al., Phys. Rev. C 100 (2019) 024314.
- [23] C. Droste, S.G. Rohozinski, K. Starosta, L. Prochniak, E. Grodner, Eur. Phys. J. A 42 (2009) 79.
- [24] Q.B. Chen, J.M. Yao, S.Q. Zhang, B. Qi, Phys. Rev. C 82 (2010) 067302.
- [25] I. Hamamoto, Phys. Rev. C 88 (2013) 024327.
- [26] J. Peng, Q.B. Chen, Phys. Lett. B 793 (2019) 303.
- [27] D.L. Balabanski, M. Danchev, D.J. Hartley, L.L. Riedinger, O. Zeidan, J.-y. Zhang, C.J. Barton, C.W. Beausang, M.A. Caprio, R.F. Casten, et al., Phys. Rev. C 70 (2004) 044305.
- [28] E.A. Lawrie, P.A. Vymers, J.J. Lawrie, C. Vieu, R.A. Bark, R. Lindsay, G.K. Mabalala, S.M. Maliage, P.L. Masiteng, S.M. Mullins, et al., Phys. Rev. C 78 (2008) 021305(R).
- [29] P.L. Masiteng, E.A. Lawrie, T.M. Ramashidzha, R.A. Bark, B.G. Carlsson, J.J. Lawrie, R. Lindsay, F. Komati, J. Kau, P. Maine, et al., Phys. Lett. B 719 (2013) 83.
- [30] P.L. Masiteng, E.A. Lawrie, T.M. Ramashidzha, J.J. Lawrie, R.A. Bark, R. Lindsay, F. Komati, J. Kau, P. Maine, S.M. Maliage, et al., Eur. Phys. J. A 50 (2014) 119.
- [31] P.L. Masiteng, A.A. Pasternak, E.A. Lawrie, O. Shirinda, J.J. Lawrie, R.A. Bark, S.P. Bvumbi, N.Y. Kheswa, R. Lindsay, E.O. Lieder, et al., Eur. Phys. J. A 52 (2016) 28.
- [32] J. Peng, J. Meng, S.Q. Zhang, Phys. Rev. C 68 (2003) 044324.
- [33] T. Koike, K. Starosta, I. Hamamoto, Phys. Rev. Lett. 93 (2004) 172502.
- [34] S.Q. Zhang, B. Qi, S.Y. Wang, J. Meng, Phys. Rev. C 75 (2007) 044307.
- [35] B. Qi, S.Q. Zhang, J. Meng, S.Y. Wang, S. Frauendorf, Phys. Lett. B 675 (2009) 175.
- [36] E.A. Lawrie, O. Shirinda, Phys. Lett. B 689 (2010) 66.
- [37] O. Shirinda, E.A. Lawrie, Eur. Phys. J. A 48 (2012) 118.
- [38] Q.B. Chen, B.F. Lv, C.M. Petrache, J. Meng, Phys. Lett. B 782 (2018) 744.
- [39] Q.B. Chen, K. Starosta, T. Koike, Phys. Rev. C 97 (2018) 041303(R).
- [40] Q.B. Chen, J. Meng, Phys. Rev. C 98 (2018) 031303(R).
- [41] Y.Y. Wang, S.Q. Zhang, P.W. Zhao, J. Meng, Phys. Lett. B 792 (2019) 454.
- [42] Q.B. Chen, N. Kaiser, U.-G. Meißner, J. Meng, Phys. Rev. C 99 (2019) 064326.

- [43] J. Meng (Ed.), Relativistic Density Functional for Nuclear Structure, International Review of Nuclear Physics, vol. 10, World Scientific, Singapore, 2016.
- [44] E.O. Lieder, R.M. Lieder, R.A. Bark, Q.B. Chen, S.Q. Zhang, J. Meng, E.A. Lawrie, J.J. Lawrie, S.P. Bvumbi, N.Y. Kheswa, et al., Phys. Rev. Lett. 112 (2014) 202502.
- [45] C.M. Petrache, Q.B. Chen, S. Guo, A.D. Ayangeakaa, U. Garg, J.T. Matta, B.K. Nayak, D. Patel, J. Meng, M.P. Carpenter, et al., Phys. Rev. C 94 (2016) 064309.
- [46] P.W. Zhao, Z.P. Li, J.M. Yao, J. Meng, Phys. Rev. C 82 (2010) 054319.
- [47] J. Peng, J. Meng, P. Ring, S.Q. Zhang, Phys. Rev. C 78 (2008) 024313.
- [48] P. Ring, P. Schuck, The Nuclear Many Body Problem, Springer Verlag, Berlin, 1980.
- [49] F.Q. Chen, Q.B. Chen, Y.A. Luo, J. Meng, S.Q. Zhang, Phys. Rev. C 96 (2017) 051303(R).
- [50] Q.B. Chen, J. Meng, Phys. Rev. C 98 (2018) 031303(R).
- [51] E. Streck, Q.B. Chen, N. Kaiser, U.-G. Meißner, Phys. Rev. C 98 (2018) 044314.
- [52] Q.B. Chen, S. Frauendorf, C.M. Petrache, Phys. Rev. C 100 (2019) 061301(R).